Chapter 9

Comparative Analysis of DFIG Based Wind Farms Control Mode on Long-Term Voltage Stability

Rafael Rorato Londero, João Paulo A. Vieira and Carolina de M. Affonso

Additional information is available at the end of the chapter

http://dx.doi.org/10.5772/52690

1. Introduction

The wind energy industry is experiencing a strong growth in most countries in the last years. Several technical, economic and environmental benefits can be attained by connecting wind energy to distribution systems such as power loss reduction, the use of clean energy, postponement of system upgrades and increasing reliability. The doubly fed induction generator (DFIG) is currently the most commonly installed wind turbine in power systems. DFIG can be operated in two different control modes: constant power factor and voltage control. In the power factor control mode, the reactive power from the turbine is controlled to match the active power production at a fixed ratio. When terminal voltage control is employed, the reactive power production is controlled to achieve a target voltage at a specified bus. Many wind operators currently prefer the unity power factor mode since it is the active power production that is rewarded [1].

The integration of wind turbine in electricity networks still face major challenges with respect to various operational problems that may occur, especially under high penetration level [2,3]. Among many problems, it can be highlighted the voltage instability phenomenon, a constant concern for modern power systems operation [4,5]. Voltage stability refers to system ability to keep voltage at all buses in acceptable ranges after a disturbance. This phenomenon is local and non-linear, characterized by a progressive decline in voltage magnitudes, and occurs basically due to system inability to meet a growing demand for reactive power at certain buses in stressed situations [6,7]. The phenomena involved in voltage stability is usually of slow nature (minutes or hours), being driven by the action of discrete type devices and load variations [7].

Some papers have analyzed the impacts caused by the connection of wind generation on voltage stability using static models [8,9]. However, the exclusive use of static models is insufficient to fully describe voltage instability phenomenon, especially considering the actuation of dynamics equipments. Also, few papers have explored the differences in DFIG mode of operation [10,11,12]. Until now, no work has presented a study analyzing the impacts of different DFIG control modes on long-term voltage stability analysis, especially considering the dynamics aspects and interaction of equipments installed in the network, such as Over Excitation Limiters (OEL) and On Load Tap Changers (OLTC).

This chapter presents a study comparing the impacts caused by different control modes of DFIG wind turbine on long-term power system voltage stability. The study uses time domain simulations and also includes the representation of Over Excitation Limiter (OEL) and On Load Tap Changers (OLTC). The analysis focuses on the two DFIG excitation control modes: constant voltage control and constant power factor control (unity power factor and leading power factor) with a 20% load increase. The impact of each control strategy is studied and the resulting change in long-term system stability is quantified, as well as the interaction between OLTC and OEL equipments.

2. Doubly Fed Induction Generators (DFIGs)

Doubly-fed induction generators are gaining popularity these days for several reasons. The primary reason for this is their ability to vary their operating speed, typically +/- 30% around the synchronous speed. The stator is directly connected to the grid and the rotor is fed from a back-to-back AC/DC/AC converter set as shows Fig. 1. The rotor side converter (RSC) controls the wind turbine output power and the voltage measured at the grid side. The grid side converter (GSC) regulates the DC bus voltage and interchange reactive power with the grid, allowing the production or consumption of reactive power. Then, DFIG can operate on voltage control mode (PV) or power factor control mode (PQ).

PV mode refers to DFIG generating or absorbing reactive power (MVAr) to/from the distribution network in order to maintain the terminal voltage at a specified value. The minimum and maximum MVAr have to be specified in order to operate at a power factor between 0.9 leading and 0.85 lagging, otherwise the plant operators will be charged for violating the operational limit. In load flow studies DFIG is represented as a PV bus for voltage control mode [13].

PQ mode refers to the DFIG generation at a fixed MW and a fixed MVAr. When DFIG real power generation varies, the reactive power will also vary to maintain a fixed power factor. This mode usually employs unity power factor operation (zero reactive power output). However, other power factor values can be specified (e.g., from 0.95 leading to 0.95 lagging) according to the system operator requirements. In load flow studies DFIG is represented as a PQ bus for power factor control mode. In this study both control modes are considered.

http://dx.doi.org/10.5772/52690

3. System modelling

3.1. Wind turbine model

The wind turbine mechanical power may be calculated as:

$$P_{mec} = 0.5 C_P \rho \, r^2 U_W^3 \tag{1}$$

Where r is the radius of the wind turbine rotor, U_w is the average wind speed (m/s), $\rho$is the air-specific mass (kg m3) and C_P is the wind turbine power coefficient [12]. C_P is a function of the tip speed ratio λ and the blade pitch angle β, and can be expressed as:

$$C_p(\lambda, \beta) = 0.73\left(\frac{115}{\lambda_i} - 0.58\beta^{2.14} - 13.2\right)e^{\frac{-18.4}{\lambda_i}} \tag{2}$$

$$\lambda = \frac{1}{\frac{1}{\lambda} - 0.02\beta + \frac{0.003}{\beta^3 + 1}} \tag{3}$$

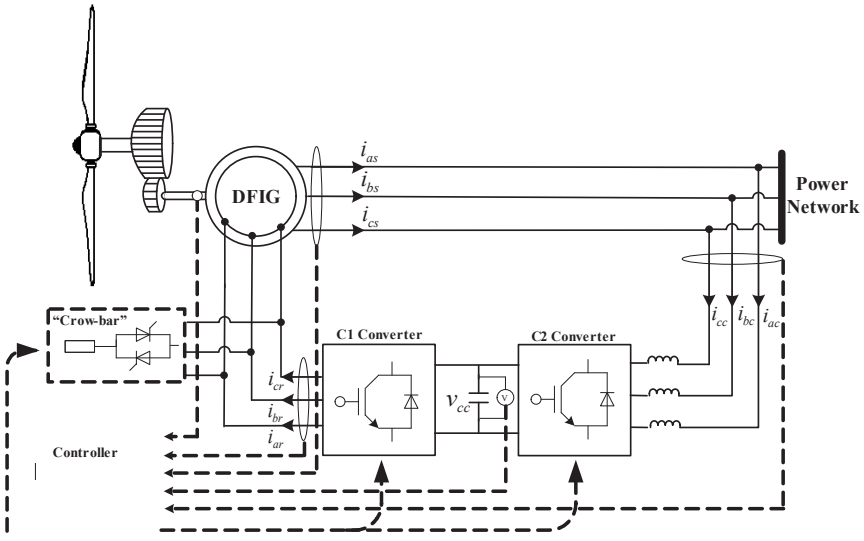

Figure 1. DFIGs Scheme

To represent the electrical and mechanical interaction between the electrical generator and wind turbine in transient stability studies, the global mass model is presented:

$$\frac{d\bar{\omega}_r}{dt} = \frac{1}{2H_T}\left(T_m - \bar{T}_e - \bar{D}\bar{\omega}_r\right) \tag{4}$$

Where $\bar{D}$ is the damping coefficient; and H_T is the inertia constant, in seconds.

3.2. The DFIG model

For power system stability studies, the generator may be modeled as an equivalent voltage source behind a transient impedance. Since the stator dynamic are very fast, when compared with the rotor ones, it is possible to neglect them. The differential equations of the induction generator rotor circuits with equivalent voltage behind transient impedance as state variables can be given in a d-q reference frame rotating at synchronous speed. For adequately representing the DFIG dynamics the second order model of the induction generator is used in the following per-unit form [14,15]:

$$\bar{v}_{ds} = -\bar{R}_s\bar{i}_{ds} + \bar{X}'\bar{i}_{qs} + \bar{e}_d' \tag{5}$$

$$\bar{v}_{qs} = -\bar{R}_s\bar{i}_{qs} - \bar{X}'\bar{i}_{ds} + \bar{e}_q' \tag{6}$$

$$\frac{d\bar{e}_d'}{dt} = -\frac{1}{T_o'}\cdot\left[\bar{e}_d' - \left(\bar{X} - \bar{X}'\right)\bar{i}_{qs}\right] + s\omega_s\bar{e}_q' - \omega_s\frac{\bar{L}_m}{\bar{L}_{rr}}\bar{v}_{qr} \tag{7}$$

$$\frac{d\bar{e}_q'}{dt} = -\frac{1}{T_o'}\cdot\left[\bar{e}_q' + \left(\bar{X} - \bar{X}'\right)\bar{i}_{ds}\right] - s\omega_s\bar{e}_d' + \omega_s\frac{\bar{L}_m}{\bar{L}_{rr}}\bar{v}_{dr} \tag{8}$$

Where:

V_{ds}, V_{qs}: d and q axis stator voltages;

R_s: stator resistance;

X′, X: transient reactance and the open circuit reactance;

i_{ds}, i_{qs}: d and q axis stator currents;
e_d',e_q': d-axis and q-axis components of the internal voltage; T_o': open circuit time constant in seconds;

ω_S: synchronous speed;

L_m: mutual inductance;

L_{rr}: rotor inductance;

V_{dr}, V_{qr}: d and q axis rotor voltages;

http://dx.doi.org/10.5772/52690

The components of the internal voltage behind the transient reactance are defined as:

$$\bar{e}_d^{'} = -\frac{\bar{\omega}_s \bar{L}_m}{\bar{L}_{rr}} \cdot \bar{\lambda}_{qr} \tag{9}$$

$$\bar{e}_q^{'} = \frac{\bar{\omega}_s \times \bar{L}_m}{\bar{L}_{rr}} \cdot \bar{\lambda}_{dr} \tag{10}$$

where λ_{qr} and λ_{dr} are d and q rotor fluxes. The reactances and transients open-circuit time constant are given:

$$\bar{X}^{'} = \bar{\omega}_s \left(\bar{L}_{ss} - \frac{\bar{L}_m^2}{\bar{L}_{rr}} \right) = \bar{X}_s + \frac{\bar{X}_r \bar{X}_m}{\bar{X}_r + \bar{X}_m} \tag{11}$$

$$\bar{T}_o^{'} = \frac{\bar{L}_r + \bar{L}_m}{\bar{R}_r} = \frac{\bar{L}_{rr}}{\bar{R}_r} \tag{12}$$

$$\bar{X} = \bar{\omega}_s \bar{L}_{ss} \tag{13}$$

$$T_o^{'} = \frac{\bar{L}_{rr}}{2\pi f_{base} \bar{R}_r} \tag{14}$$

3.3. DFIG converter model

In this study the converters are modeled according to reference [16], as show the diagrams presented in Figs. 2 and 3. The V_{d1} component is used to the capacitor voltage and V_{q1} is used to fix at zero the reactive power absorbed by the rotor side converter. This component may be used to provide additional reactive power support to the system.

The component I_{q2} of the rotor current is used to control the rotor speed and as a consequence, the active power supplied by the machine. The component I_{d2} of the rotor current is used to control the generator terminal voltage or power factor.

3.4. OEL model

The objective of the over excitation limiter is to protect the generator from thermal overload. The OEL model adopted in this study is the same of reference [14] and the model is presented in Fig. 4. The OEL detects the over-current condition, and after a time delay, acts reducing the excitation by reducing the field current to a value of 100% to 110% of the nominal value. Once the OEL acts, the field current no longer increases, limiting the reactive power supplied by the machine to a minimum value, overloading the other generators, contributing significantly to the voltage instability.

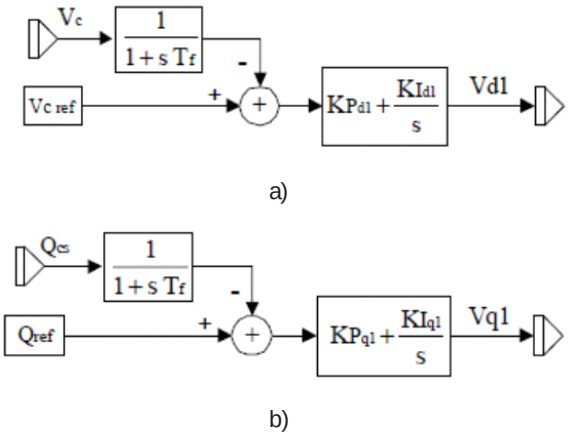

Figure 2. Control loop of the stator side converter (SSC) a) Component V_{d1} b) Component V_{q1}.

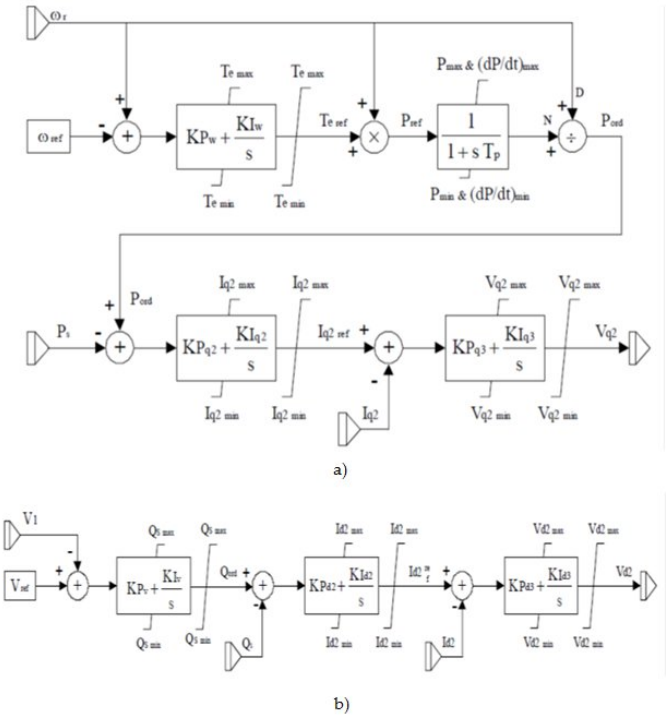

Figure 3. Control loop of the rotor side converter (RSC) a) Component I_{q2} b) Component I_{d2}.

http://dx.doi.org/10.5772/52690

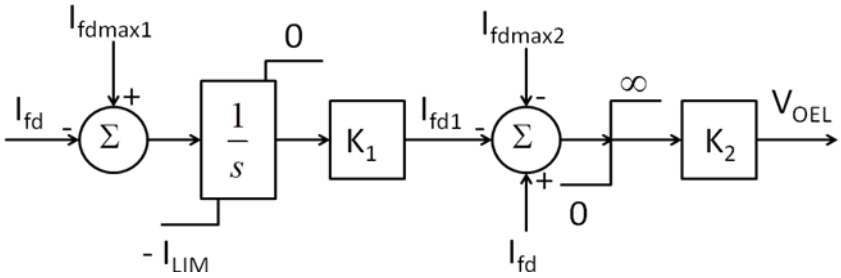

Figure 4. OEL model.

4. Test system

The test system used in this study is shown in Fig. 5 and is based on the system developed in [14] for voltage stability analysis. To conduct this study the original system was modified, adding a transformer between buses 8 and 12 to connect a 212.5 MW wind farm at bus 12, consisting of 250 turbines of 850kW. Four generation sources are modeled: G1, G2 and G3 are synchronous generators and the wind farm is based on DFIG. The OEL device is installed in generator G3 and the OLTC between buses 10 and 11. The OLTC model used is presented in reference [17].

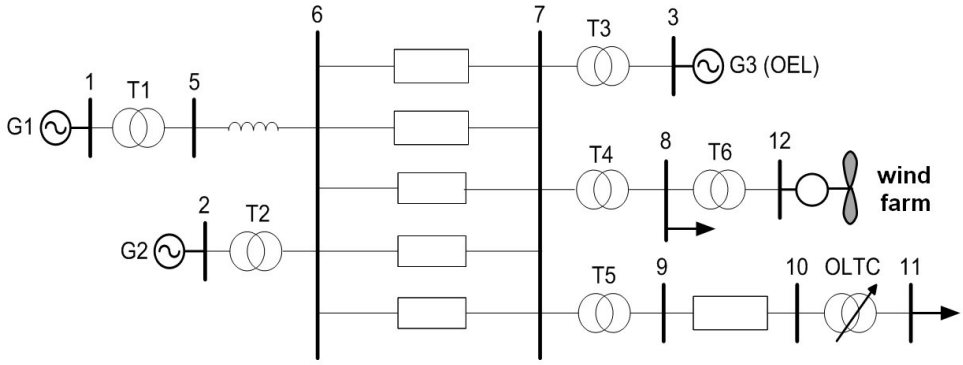

Figure 5. Test system diagram.

Table 1 shows the generation and load scenarios considered. The penetration level of the wind farm is 17.6%. Scenario 1 considers the load at bus 8 modeled as constant impedance for both active and reactive components and the load at bus 11 modeled as 50% constant impedance and 50% constant current for both active and reactive components. Scenario 2 considers the active power component of load at bus 8 represented as an equivalent of 450

induction motors which parameters are presented in the Appendix, and all other components are modeled as in scenario 1.

Scenarios	Load at bus 8		Load at bus 11	
	P(MW)	Q(Mvar)	P(MW)	Q(Mvar)
Scenario 1	3,271.0	1,015.0	3,385.0	971.3
Scenario 2	1,660.0	1,050.2	3,388.4	972.3

Table 1. Load Scenarios

Scenarios	Generator 1 (MW)	Generator 2 (MW)	Generator 3 (MW)	DFIG (PV mode) (MW/Mvar)	DFIG (PQ mode) (MW/Mvar)
Scenario 1	2,747.0	1,736.0	1,154.0	1,200.0 / -364.0	1,200.0 / 100.0
Scenario 2	1,115.5	1,736.0	1,154.0	1,200.0 / -14.3	1,200.0 / 200.0

Table 2. Generation Scenarios

The intermittent characteristic of wind generation is considered following the wind regime presented on Fig. 6, with the initial wind speed of 12 m/s.

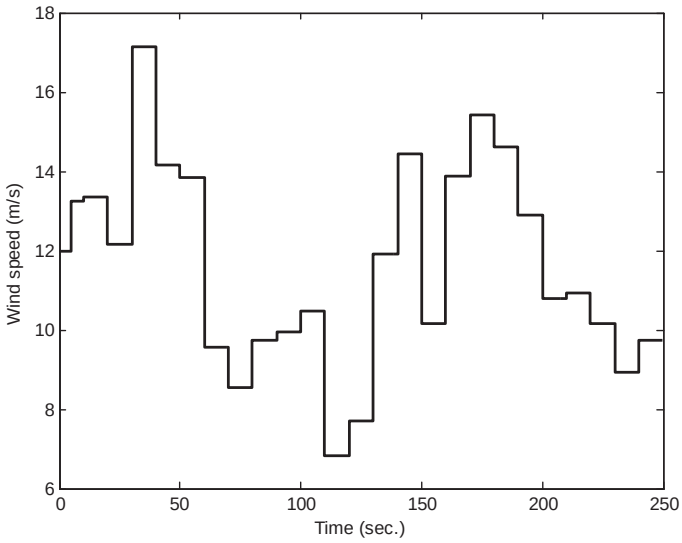

Figure 6. Wind speed regime.

http://dx.doi.org/10.5772/52690

5. Simulation and results

To evaluate the different impacts caused by DFIG control modes on long-term voltage stability, two cases are analyzed:

- Case A: Static load model (scenario 1): This scenario considers the load at buses 8 and 11 represented by the commom ZIP model.
- Case B: Static and dynamic load model (scenario 2): This scenario considers the load at bus 11 represented by the common ZIP model and the active power component of load at bus 8 represented by an equivalent induction motor.

All simulations considered both DFIG control modes alternatively: power factor control mode (0.99 leading) and voltage control mode. The results and analysis are presented next in the following sections. The simulations were conducted using the softwares ANAREDE for load flow calculations and ANATEM for transient stability simulations [18,19].

5.1. Case A: Static load model (Scenario 1)

This case considers the successive increase on system total demand, with increments of 0.1% every second in respect with the initial load from scenario 1 as presented in tables 1 and 2. The load increases up to 200 seconds and the simulation time is 250 seconds.

As load increases, the voltage at bus 11 decreases, causing OLTC to operate in order to maintain voltage close to the reference level for both control modes as shows Fig. 7. However, while OLTC improves voltage level at bus 11, it progressively depresses voltage at bus 8 with each tap-changing operation, mainly when power factor control mode is employed in wind generation as shows Fig. 8. In voltage control mode, DFIG maintain the voltage level at bus 8 with its capacity to supply reactive power support. Fig. 9 presents the reactive power injected and absorbed by DFIG. Note that when OLTC starts to operate close to 60 seconds, the DFIG starts to inject more reactive power in the system until it reaches its maximum limit.

The voltage reductions at load buses 8 and 11 are directly reflected in the field current of generator 3, because with the load increase, the generator AVR (Automatic Voltage Regulator) would quickly restore terminal voltage by increasing excitation, which results in additional reactive power flow through the inductances of transformers and lines, causing increased losses and voltage drops. At this stage, generator G3 tends to reach its field current limit with the load ramp increase as shows Fig. 10. In this scenario 1, generator 3 does not suffer over-excitation (the OEL is not activated), and the long-term power system voltage stability is maintained in both reactive power control modes, at least apparently. However, as can be seen in Fig. 10, the DFIG's voltage control mode has a positive effect in the power system voltage stability since it tends to delay the OEL operation because the field current level is smallest from 110 s up to 250 s, providing less risk of protection interventions and system security degradation.

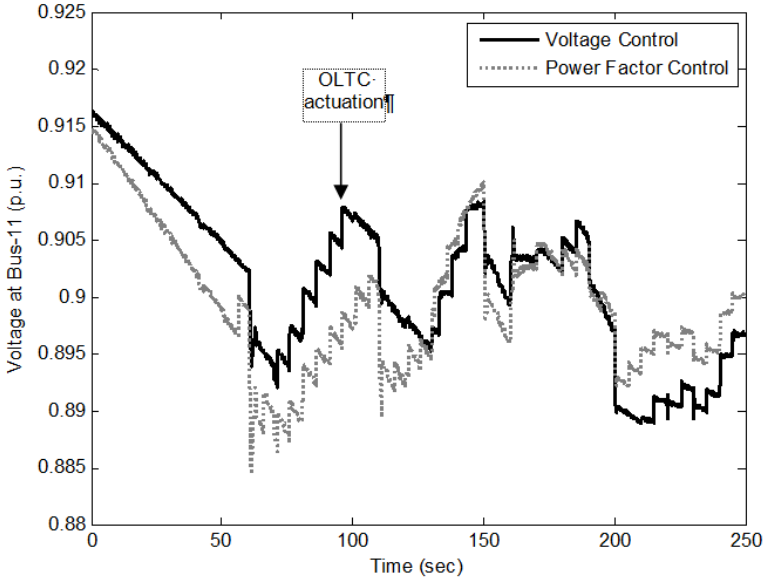

Figure 7. Voltage at bus 11

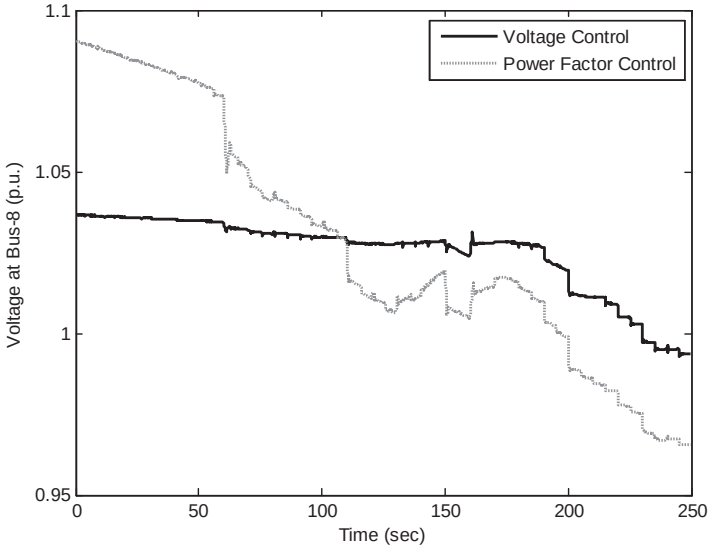

Figure 8. Voltage at bus 8

http://dx.doi.org/10.5772/52690

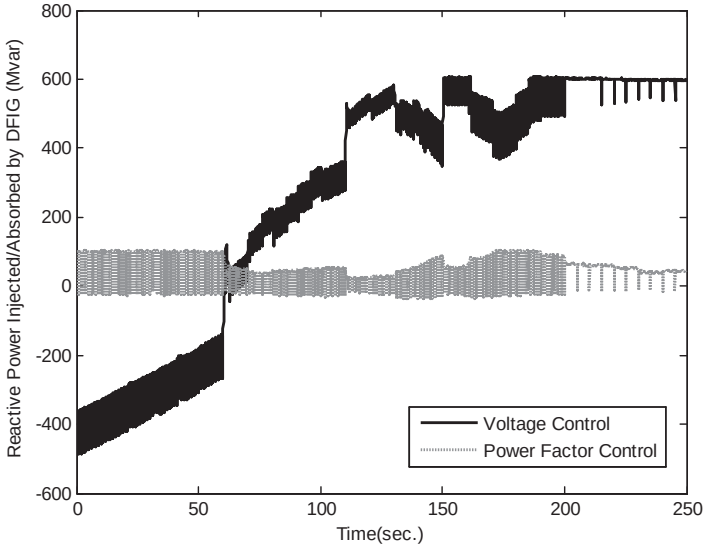

Figure 9. Reactive power injected / absorbed by DFIG.

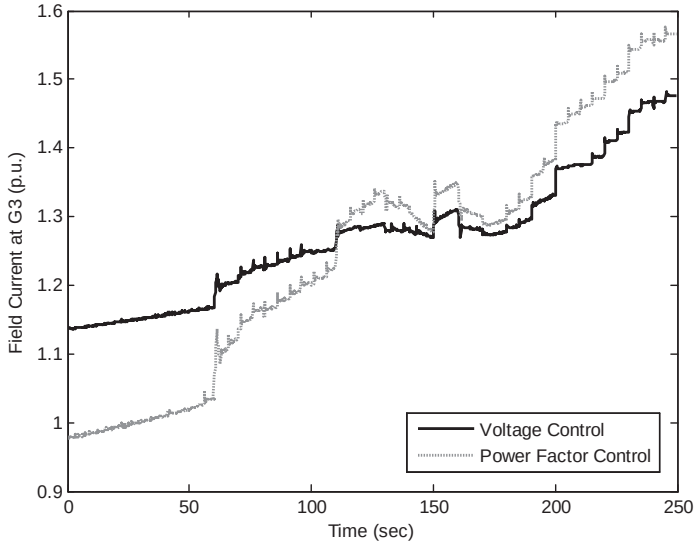

Figure 10. Field current at G3.

Fig. 11 shows the OLTC behavior during the load ramp increase. The results show that the OLTC reaches its upper limit when the DFIG wind generators are configured to control the power factor, and in this case the wind turbines cannot provide reactive power to support the voltages in the system. On the other hand, when the voltage control mode is used, the OLTC does not reach the upper tap limit, increasing the long term voltage stability margin.

Fig. 12 shows the system PV curve when DFIG is operating in both power factor and voltage control modes. These curves were obtained by increasing the load and plotting the voltage at bus 8 considering the dynamic aspect of the equipments in the system. This curve indicates the maximum loadability point, which is the maximum power the system can provide. The results show that when DFIG is operating in voltage control mode it increases significantly the maximum loadability point (nose point), since this equipment can supply reactive power to the system through voltage control. It is important to mention that the PV curves contours are irregular since they represent the discrete actuation of OEL and OLTC.

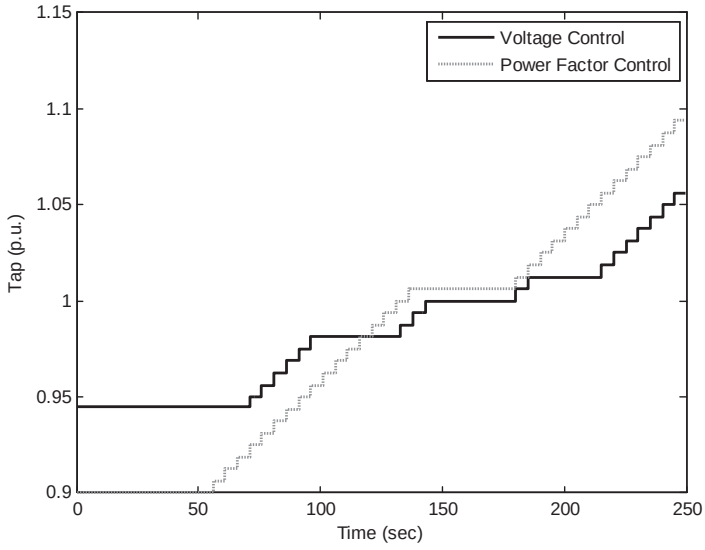

Figure 11. Tap position.

http://dx.doi.org/10.5772/52690

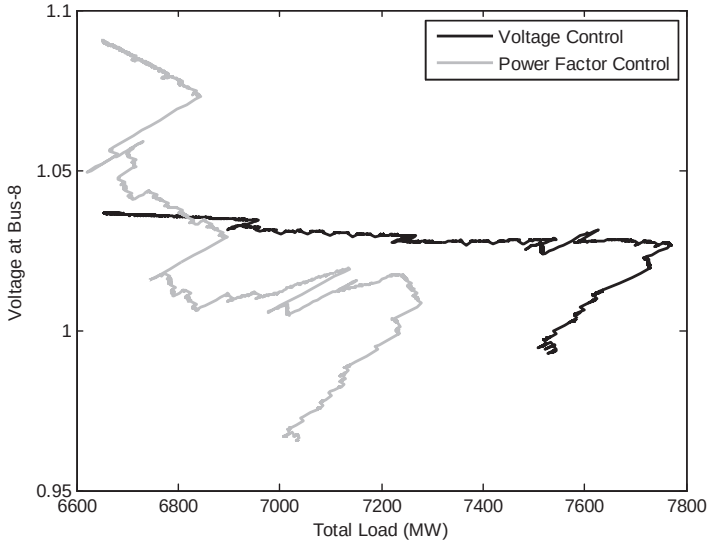

Figure 12. PV curve at bus 8.

5.2. Case B: Static and dynamic load models (Scenario 2)

This case considers the successive increase on system demand from bus 11, with increments of 0.1% every second in respect to the initial load from scenario 2 as presented in tables 1 and 2. The load increases up to 200 seconds and the simulation time is 250 seconds.

As seen in Figs. 13 and 14, the power factor control mode results in a heavy reactive power demand from the power system, leading to a very low voltage profile at load buses 11 and 8. In this case, constant power factor strategy decreases the long-term voltage stability margin, resulting in the voltage deterioration at load buses caused by relevant effect of the OEL combined with the OLTC action. In voltage control mode, the DFIG maintain the voltage level at bus 8 with its capacity to supply reactive power to the grid, as shows Fig. 15.

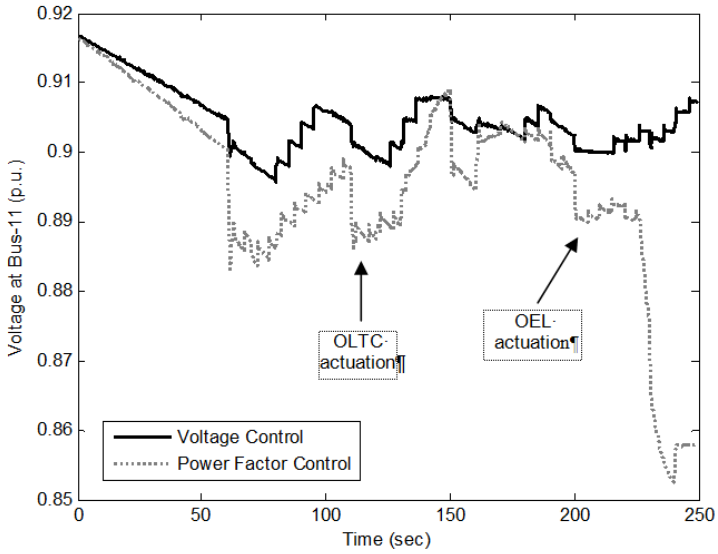

Figure 13. Voltage at Bus 11.

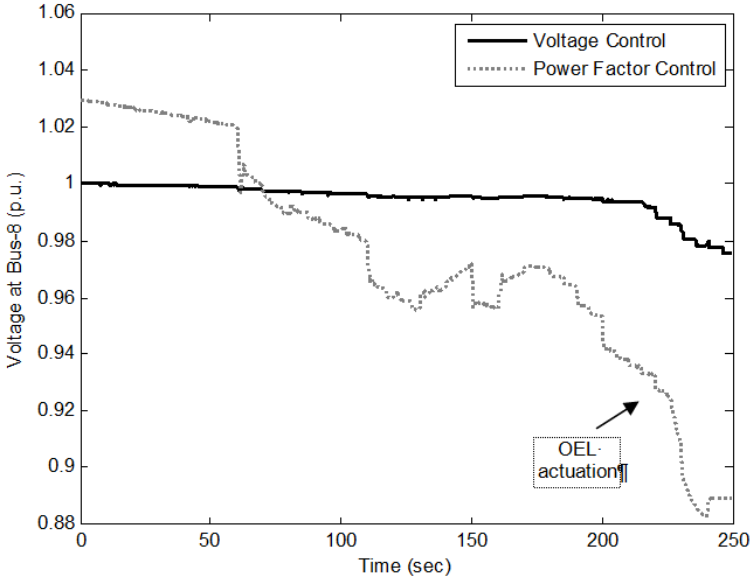

Figure 14. Voltage at Bus 8.

http://dx.doi.org/10.5772/52690

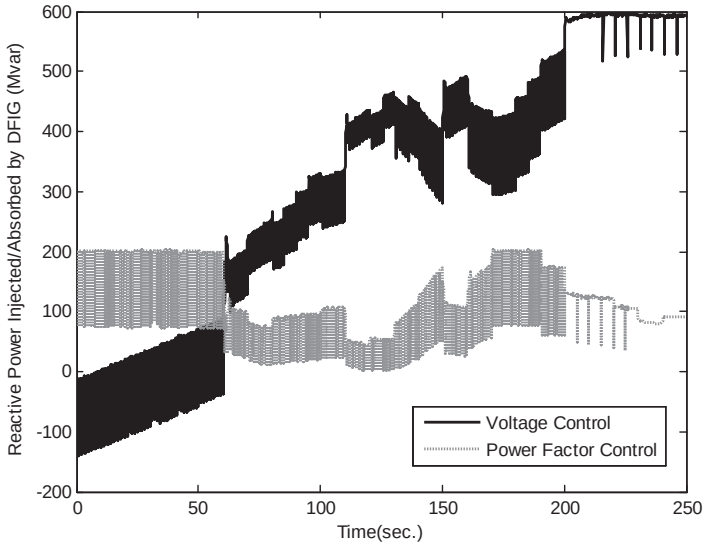

Figure 15. Reactive power injected / absorbed by DFIG.

Fig. 16 shows the field current behavior from generator 3. The DFIG's power factor control mode increases the field current demand and the OEL begins to operate at 225 s reducing the current, and as a consequence, the reactive power injected by G3 decreases.

On the other hand, when the DFIG is operating with voltage control mode the OEL is not activated, increasing the voltage stability margin. The DFIG's voltage control mode demonstrates that can be utilized in order to improve the long-term voltage stability in a system with a high wind penetration. From these results, one can conclude that the DFIG's voltage control mode has a beneficial effect in the voltage stability when the power system is submitted to load increase, considering the dynamic aspects of the OEL and OLTC combined with the load characteristics adopted. It is important to highlight that load characteristics and power system voltage control devices are among key factors influencing voltage stability.

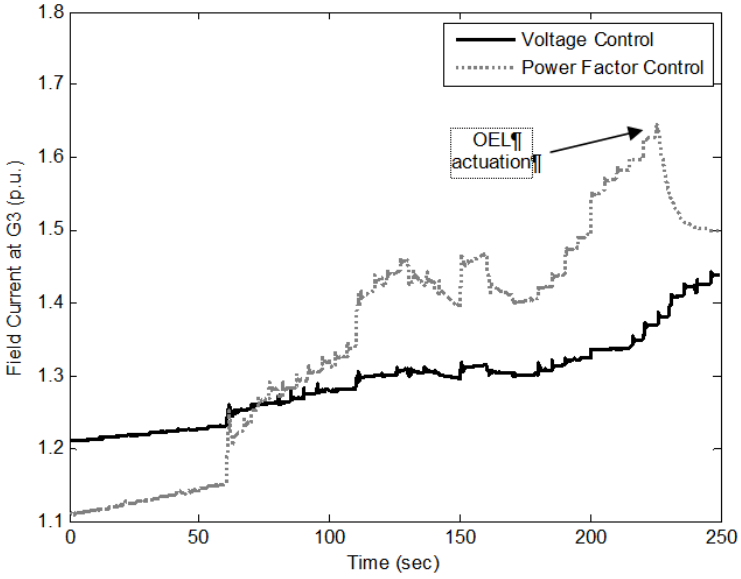

Figure 16. Field Current from G3.

Fig. 17 shows the OLTC behavior during the load ramp increase. It is observed that the minimum and maximum tap positions are reached when the DFIG wind turbines are configured to control the power factor, in order to support the voltage at bus 11. This is a great disadvantage of power factor control mode. The reactive power system reserves are insufficient and the OLTC tap changing is detrimental to voltage profile, increasing the risk of long-term voltage instability.

On the other hand, the voltage control strategy provides a delay on the OLTC actuation. Besides, the OLTC does not even reach the upper tap limit. When the OLTC is not changing its tap position, the reactive power absorbed decreases as well as the transmission line losses, causing a smallest drop in voltages. In this case, the power system is much more prone to maintain the voltage stability.

http://dx.doi.org/10.5772/52690

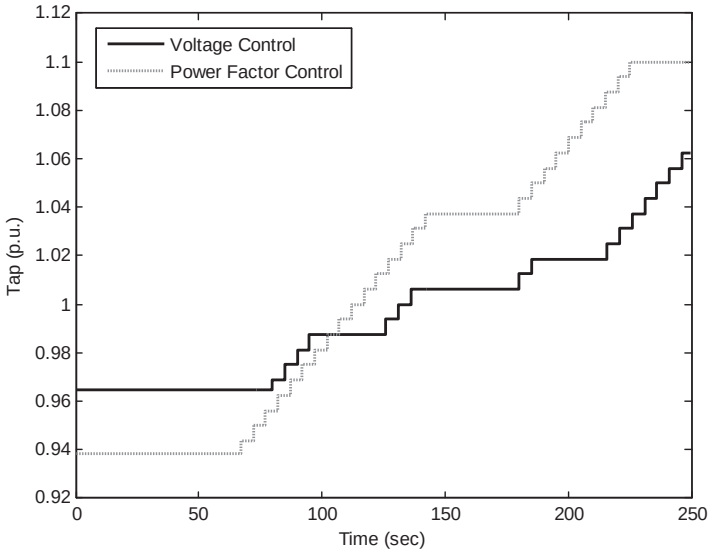

Figure 17. Tap position.

The DFIG's terminal voltage control mode based on the rotor excitation current allows the maintenance of reactive power consumed by the motor as shows Fig. 18. In this case, there are no extra static or dynamic reactive compensation demands for maintaining the power system long-term voltage stability. On the other hand, the DFIG's power factor control mode causes an increase in the reactive power drawn by the motor, which is necessary to maintain the power system reactive power balance. In this case, the motor is subject to a sudden stall that can cause a voltage collapse manifested as a slow decay of voltage in a significant part of the power system.

Fig. 19 shows the system PV curve for both DFIG control modes. In this case, the maximum loadability points for voltage and power factor control modes don't show much difference between each other as the previous case (static load). This occurs since in this case the load is incremented only at bus 11, which is controlled by the OLTC. Then, the active power absorbed at bus 8 shows only a small drop, which is reflected to the PV curve. The load at bus 8 (motors) was not incremented because the motor would consume too much reactive power from the system.

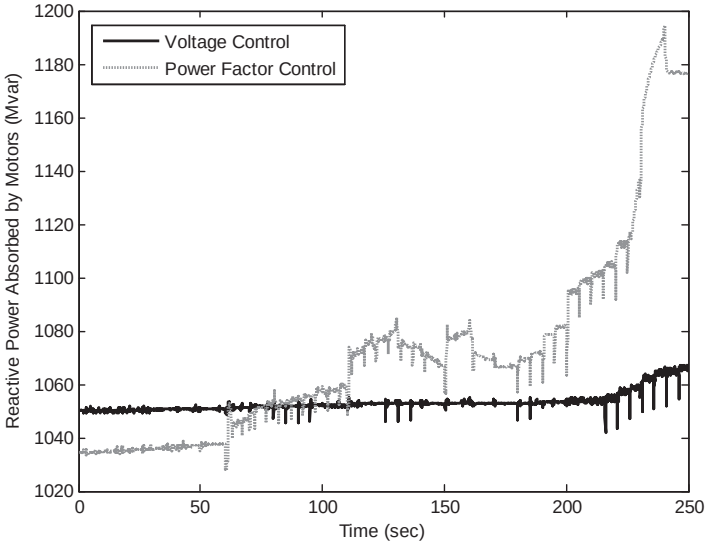

Figure 18. Reactive power absorbed by the motors.

http://dx.doi.org/10.5772/52690

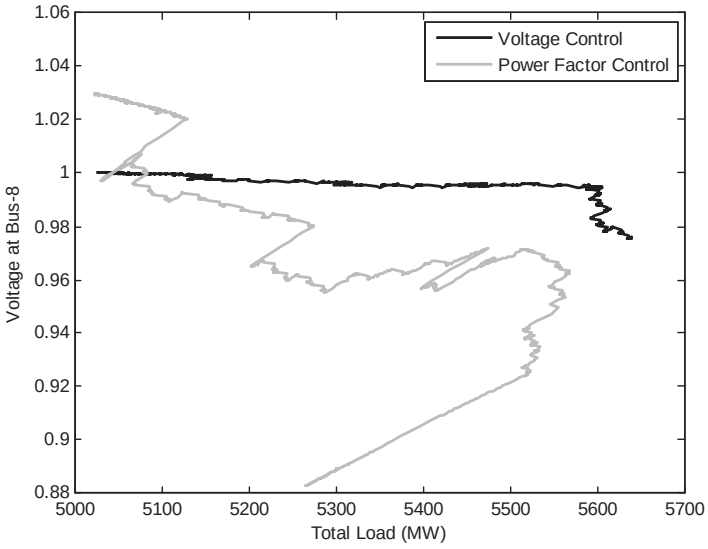

Figure 19. PV curve at bus 8.

6. Conclusion

This paper presented studies analyzing the impacts of different control strategies from DFIG wind turbines on power system long-term voltage stability by time domain simulations. The study considered the dynamic models of generator OEL and OLTC transformer combined with static and dynamic load representations. The simulation results confirm the expectation that when DFIG operates in power factor control mode the voltage stability margin is poor, mainly when the motor model is used to represent a part of the load. The results clearly show that DFIG's voltage control mode enhances voltage stability margin. The voltage control is more robust than power factor control when the power system is subjected to a slow load increase, a process that involves the OEL and OLTC actions and interactions. The use of DFIG in voltage control mode also increased the maximum loading point as well as delayed the OEL and OLTC actuation, helping to avoid problems of voltage collapse in the power system. As part of the ancillary services, the voltage control mode may have an increasing market ahead. This is an important feature that must be considered in the choice of the control strategy to be used on DFIG wind turbines.

Appendix

Generators 1, 2 and 3 parameters (p.u. on base of machine rating):

$R_a = 0.0046 X_d = 2.07 X'_d = 0.28 X''_d = 0.215$

$X_q = 1.99 X'_q = 0.49 X''_q = 0.215 X_l = 0.155$

$T'_{d0} = 4.10\ s T'_{q0} = 0.56\ s$

$T''_{d0} = 0.033 s T''_{q0} = 0.0062\ s$

G2: H = 2.09s, S_b = 2200 MVA

G3: H = 2.33s, S_b = 1400 MVA

SCIG and DFIG parameters (on base of machine rating):

$r_s = 0.85\% X_s = 5.776\% X_m = 505.9\%$

$r_r = 0.712\% X_r = 8.094\% H = 3.5\ s$

Poles = 2Power = 1140 HP

DFIG wind turbine parameters:

Rotor diameter = 58 mGear ratio = 74.5

DFIG power curve:

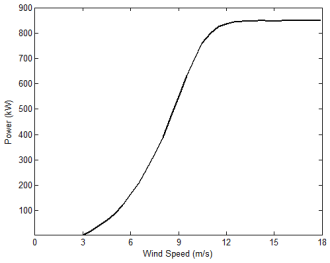

OLTC parameters:

Time delay for the first tap movement = 30 s

Time delay for subsequent tap movement = 5 s

Dead band = ±1% bus voltage

Tap range = ±16 steps

Step size = 5/8% (0.00625 pu)

Induction Motor parameters (p.u. on base of machine rating):

$X_m = 3.3\ R_s = 0.01 X_s = 0.145$

$R_r = 0.008 X_r = 0.145$

H = 0.6s, 4,826.0 HP

Generic network parameters (p.u. on base S_b = 100MVA):

Line 5-6:R = 0.0 X = 0.0040B = 0.0

Line 6-7:R = 0.0015 X = 0.0288B = 1.173

Line 9-10: R = 0.0010X = 0.0030B = 0.0

T1:R = 0.0X = 0.0020Ratio = 0.8857

T2: R = 0.0X = 0.0045Ratio = 0.8857

T3:R = 0.0 X = 0.0125Ratio = 0.9024

T4:R = 0.0 X = 0.0030Ratio = 1.0664

T5:R = 0.0 X = 0.0026Ratio = 1.0800

http://dx.doi.org/10.5772/52690

Author details

Rafael Rorato Londero, João Paulo A. Vieira and Carolina de M. Affonso

Faculty of Electrical Engineering, Federal University of Pará, Belém, PA, Brazil

References

[1] Standard interconnection agreements for wind energy and other alternative technologies, Washington, DC: Federal Energy Regulatory Commission (FERC) 661-A, Dec. 2005.

[2] Jenkins N, Allan R, Crossley P, Kirschen D, Strabac G (2000) Embedded Generation, The Institution of Electrical Engineers, London, United Kingdom.

[3] Trichakis P, Taylor P C, Lyons P F, Hair R (2008). Predicting the technical impacts of high levels of small-scale embedded generators on low-voltage networks, IET Renewable Power Generation, vol. 2, no. 4, pp. 249–262.

[4] Vournas C D, Nikolaidis V C, Tassoulis A (2005). Experience from the Athens Blackout of July 12, 2004, in Proceedings of the IEEE Power Tech Conference, St Petersburg, Russia, pp. 1-7.

[5] Corsi S, Sabelli C (2004). General Blackout in Italy Sunday September 28, 2003, h. 03:28:00, in Proc. IEEE Power Engineering Society General Meeting, vol. 2, pp. 1691-1702.

[6] Taylor C (1994). Power System Voltage Stability, New York: McGraw-Hill Inc.

[7] IEEE/CIGRE Joint Task Force on Stability Terms and Definitions (2004). Definition and Classification of Power System Stability, IEEE Trans. on Power Systems, vol. 19, no. 2, pp. 1387-1401.

[8] Tapia A, Tapia G, Ostolaza J X, Saenz J R (2003). Modeling and control of a wind turbine driven doubly fed induction generator, IEEE Trans. Energy Conversion, vol. 18, no. 2, pp. 194–204.

[9] Cartwright P, Holdsworth L, Ekanayake J B, Jenkins N (2004). Coordinated voltage control strategy for a doubly-fed induction generator (DFIG)-based wind farm, in Proceedings of the IEE Generat. Transmiss. Distribution, vol. 151, no. 4, pp. 495–502.

[10] Kayıkçi M, Milanović J V (2007). Reactive Power Control Strategies for DFIG-Based Plants, IEEE Trans. on Energy Conversion, vol. 22, no. 2, pp. 389-396.

[11] Muñoz J C, Cañizares C A (2011). Comparative Stability Analysis of DFIG-based Wind Farms and Conventional Synchronous Generators, IEEE Power Systems Conference and Exposition, Phoenix, pp. 1-7.

[12] Ackermann T (2005). Wind Power in Power Systems, John Wiley & Sons Ltd..

[13] Koon L C, Abdul Majid A A (2007). Technical issues on Distributed Generation (DG) connection and guidelines, 19th International Conference on Electricity Distribution (CIRED), Vienna, pp. 1-4.

[14] Kundur P (1994). Power System Stability and Control, New York: McGraw-Hill.

[15] Anaya-Lara O, Jenkins N, Ekanayake J, Cartwright P, Hughes M (2009). Wind Energy Generation Modelling and Control, John Wiley & Sons.

[16] Ekanayaka J B, Holdsworth L, Wu X G, Jenkins N (2003). Dynamic Modeling of Doubly Fed Induction Generator Wind Turbine, IEEE Transactions on Power Systems, vol.18, no.2, pp.803-809.

[17] Rangel R D, Guimarães C H C (2007). Modelagem de Transformadores com Dispositivos de Comutação em Carga para Utilização em Programas de Simulação Dinâmica, in Proceedings of XIX Seminário Nacional de Produção e Transmissão de Energia Elétrica - SNPTEE.

[18] CEPEL, Centro de Pesquisas de Energia Elétrica (1999). ANAREDE: Programa de Análise de Redes, Manual Guide, 9.5 Version.

[19] CEPEL, Centro de Pesquisas de Energia Elétrica (2002). ANATEM: Análise de Transitórios Eletromecânicos, Manual Guide, 10 Version.